Comparison of hard and soft x-ray photoelectron spectra of silicon

F. Offi,[1] W. S. M. Werner,[2] M. Sacchi,[3] P. Torelli,[4] M. Cautero,[5] G. Cautero,[5] A. Fondacaro,[1,*] S. Huotari,[6] G. Monaco,[6] G. Paolicelli,[4] W. Smekal,[2] G. Stefani,[1] and G. Panaccione[7]

[1]*CNISM and Dipartimento di Fisica, Università Roma Tre, Via della Vasca Navale 84, I-00146 Rome, Italy*

[2]*Institut für Allgemeine Physik, Vienna University of Technology, Wiedner Hauptsraße 8-10, A-1040 Vienna, Austria*

[3]*Synchrotron Soleil, Boîte Postale 48, F-91142 Gif-sur-Yvette, France and Laboratoire de Chimie Physique-Matière et Rayonnement, Universté P. et M. Curie, UMR 7614, 11 rue P. et M. Curie, F-75005 Paris, France*

[4]*CNR-INFM-S3, Via Campi 213/A, I-41100 Modena, Italy*

[5]*Sincrotrone Trieste S.C.p.A., Strada Statale 14 km 163.5, Area Science Park, Basovizza, I-34012 Trieste, Italy*

[6]*European Synchrotron Radiation Facility, Boîte Postale 220, F-38042 Grenoble, France*

[7]*Laboratorio Nazionale TASC-INFM-CNR, Area Science Park, Basovizza Strada Statale 14 km 163.5, I-34012 Trieste, Italy*

(Received 12 October 2006; revised manuscript received 29 June 2007; published 17 August 2007)

A detailed comparison of the surface sensitivity of x-ray photoemission spectroscopy for hard and soft x rays is presented and discussed. Electron scattering parameters and their energy dependence are given for Si and two Si spectra are analyzed: a Mg $K\alpha$ ($h\nu$=1253.6 eV) excited spectrum of the Si 2*p* and 2*s* lines and a hard x-ray excited spectrum ($h\nu$=5925 eV) of the Si 1*s* line. The differential inelastic scattering characteristics for Si are extracted from reflection electron energy loss spectra taken at energies of 1500 and 4000 eV. Using these scattering characteristics and electron mean free paths from the literature, simulated spectra are compared with experiment. The experimental spectra are deconvoluted to give the true intrinsic line shape corresponding to the theoretical collision statistics when interference effects between intrinsic and extrinsic scattering are neglected. The magnitude of interference effects cannot be assessed by our analysis. Within the (unknown) uncertainty introduced by neglecting interference effects, it is possible to determine the relative intensity of intrinsic and extrinsic excitations. In this way, it is found that in the case of the soft x-ray excited photoelectron spectrum of the shallower electronic shells (2*p* and 2*s*), intrinsic plasmon creation is rather weak, and the apparent asymmetric line shape of the spectrum might be interpreted as the fact that electron-hole pair creation dominates the intrinsic loss spectrum, while an alternative explanation in terms of surface core level shifted components is also proposed. For the deeper core electronic shell, probed with hard x rays, the opposite situation is observed: while intrinsic electron-hole pair creation was not observed, a strong contribution of intrinsic plasmon losses of about 30% was seen.

DOI: 10.1103/PhysRevB.76.085422 PACS number(s): 79.60.−i, 79.20.Uv

I. INTRODUCTION

Hard x-ray photoemission electron spectroscopy (HAXPES) is a recent development in x-ray photoemission techniques that offer new capabilities for the investigation of bulk electronic properties of materials.[1] The idea behind HAXPES is that photoemission experiments at low kinetic energy ($E<500$ eV), while providing a wealth of information about electronic properties, are limited intrinsically to the investigation of surfaces, due to the small escape depth of the electrons over the considered energy range. This has generated a remarkable unbalance between our knowledge of bulk and surface electronic properties, a difficulty that is evident especially in the investigation of systems where a direct comparison between surface and bulk is mandatory, such as, for example, strongly correlated systems.[2] A straightforward way to increase the probing depth in photoemission experiments is to increase the energy of the analyzed electrons, i.e., to increase the energy of the excitation source into the hard x-ray region (>5 keV). Until recently, such a development, whose pioneering attempts were already performed in the 1970s,[3] has been mainly limited by both the intensity and energy resolution of the photon source and the performance of electron analyzers in terms of transmission and energy resolution. Indeed, one has to take into account the strong reduction in photoionization cross section with increasing photon energy.[4] The use of high flux and high energy resolution x-ray beams available at synchrotron radiation facilities, along with the recent development of dedicated electron spectrometers,[5] has turned HAXPES into a valuable tool for the investigation of bulk materials and buried interfaces.[6–11]

One of the key points in the development of photoemission from solids is a proper comparison between surface sensitive and bulk sensitive photoemission spectra. In other words, it appears to be of primary importance to quantify the information depth of HAXPES, for example, via a proper evaluation of the inelastic mean free path at high electron energies. Recently, we attempted to quantify the effective attenuation length in high energy photoemission by using the so-called overlayer method, i.e., by detecting the photoemitted electron intensity of the substrate and overlayer films as a function of the thicknesses of wedge-shaped overlayers.[12] An effective attenuation length around 45–50 and 60–65 Å has been found for electron kinetic energies around 4 and 6 keV, respectively, for materials such as Co, Cu, and Ge, while smaller values (30–35 and 45–50 Å, respectively) were found for Gd_2O_3. These results are in agreement with previously reported data on GaAs by Dallera *et al.*[8] and on Ge by Berény *et al.*[13]

In the present paper, we compare hard and soft x-ray excited photoelectron spectra from a Si sample. The surface sensitivity of these two cases is analyzed carefully and this analysis forms the basis for spectrum simulation and line shape analysis of the two spectra. The consistency between simulated and experimental spectra allows us to conclude that the surface sensitivity is well described by the employed model.

II. SURFACE SENSITIVITY OF PHOTOEMISSION SPECTROSCOPY FOR SOFT AND HARD X RAYS

The surface sensitivity of electron beam techniques is governed by the electron-solid interaction. The strength of the interaction decreases with increasing electron speed, giving rise to larger mean free paths at higher energies. This holds true both for the inelastic interaction with the loosely bound solid state electrons that is the dominant mechanism for energy losses as well as for the elastic interaction with the Coulomb field of the atomic nuclei that is mainly responsible for changes in the direction of motion. The distinction between elastic and inelastic scattering can be made to a good approximation since deflections in a collision with the free electrons give rise to scattering angles that are very small as a rule, while the recoil energy transfer to a nucleus in an elastic deflection is negligible compared to the energy transferred to the solid state electrons in an inelastic collision.[14] Inelastic scattering deep inside the solid is characterized by the differential inverse inelastic mean free path (DIIMFP), i.e., the distribution of energy losses in an individual collision per unit path length. The total inelastic mean free path (IMFP) λ_i determines the average distance an electron travels in between successive inelastic collisions, measured along its flight path. This quantity is displayed in Fig. 1 for silicon, along with the elastic mean free path (EMFP) λ_e, i.e., the average distance between elastic collisions and the so-called transport mean free path (TrMFP) λ_{tr} that is the typical distance traversed in between large angle deflections and is the characteristic length for momentum relaxation.

Since the mean free path for interaction increases with increasing energy, the average depth from which the signal electrons can escape without inelastic scattering increases for hard x-ray photoemission. However, the absolute value of the interaction characteristics does not convey all details concerning the surface sensitivity since the surface sensitivity is governed by the combined influence of inelastic and elastic scattering. Under the influence of elastic scattering, the path length traveled in the solid by a signal electron starting at the depth z and escaping in an off-normal polar direction $\mu=\cos\theta$ increases and significantly exceeds the path length $l=z/\mu$ it would travel in the absence of elastic scattering. The extent of the path length elongation is a function of the so-called scattering parameter $\chi=\lambda_i/\lambda_{tr}$.[15] It is seen from Fig. 1 and Table I that this parameter depends significantly on the energy: for the typical energy range of a soft x-ray excited spectrum of about 1000 eV, the value of the scattering parameter is about $\chi\approx 0.2$, implying that on the average five energy losses take place before the electron is deflected over a large angle of the order of $\gtrsim\pi/2$ or, in other words, that the probability to experience a large angle deflection while the electron travels a distance of the order of the inelastic mean free path is equal to 0.2. For hard x-ray photoemission, the typical signal electron energy is of the order of several keV and the probability for large angle deflections in between inelastic collisions decreases significantly to about 5%. In other words, in this energy regime, the

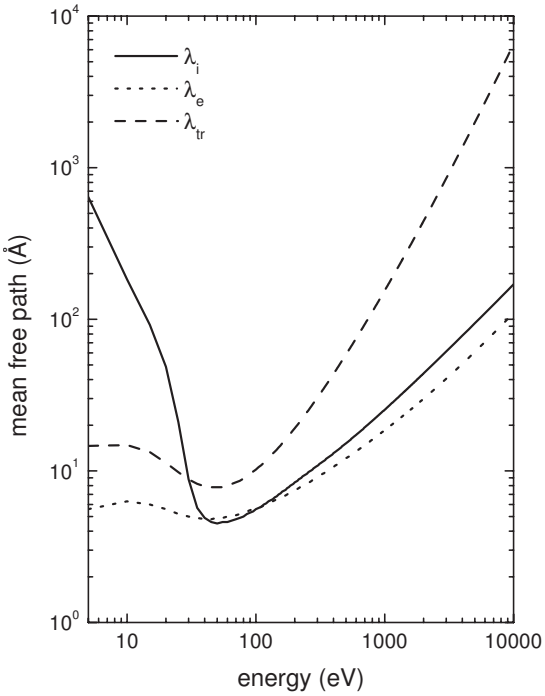

FIG. 1. Quasielastic interaction parameters for Si in the 5–10 000 eV energy range. Solid line, inelastic mean free path (IMFP, λ_i); dotted line, elastic mean free path (EMFP, λ_e); dashed line, transport mean free path (TrMFP, λ_{tr}). These data were generated using the SESSA software (Ref. 27).

TABLE I. Parameters describing the elastic and inelastic interaction for medium energy electron transport in Si. The elastic, inelastic, and transport mean free paths are denoted by λ_e, λ_i, and λ_{tr} respectively, while $\chi=\lambda_i/\lambda_{tr}$ is the scattering parameter in the quasielastic energy regime. These data were provided by the SESSA software (Ref. 27).

E (eV)	λ_e (Å)	λ_i (Å)	λ_{tr} (Å)	χ
100	5.6	5.4	9.9	0.55
200	7.4	8.2	18.6	0.44
500	12.0	15.2	57.7	0.26
1000	18.5	25.5	153.6	0.17
2000	29.8	44.3	441.9	0.10
5000	60.9	95.0	1977.7	0.05
10000	110.0	171.8	6508.2	0.03
20000	202.7	313.9	21997	0.01
30000	289.3	448.1	45033	0.009
50000	456.8	711.5	97989	0.007

straight line approximation (SLA), in which deflections of the direction of motion are altogether neglected, is a reasonable one.

Quantitatively, the influence of elastic scattering on the surface sensitivity is described by the distribution of path lengths $Q(s,\mu,z')$ for electrons starting at the depth z' and escaping from the surface in the polar direction $\mu=\cos\theta$ after traveling a path length s. Except for a few simple cases,[16,17] it is difficult to derive accurate analytical expressions for the path length distribution. Therefore, this quantity is usually calculated numerically, the Monte Carlo technique being a convenient approach for this purpose.[18] The so-called partial escape distributions or depth distribution functions (DDFs), $\phi_n(\mu,z')$, describe the surface sensitivity in photoemission and related techniques. These quantities represent the distribution of the depth of origin z' for electrons that arrive in a detector with a polar orientation $\mu=\cos\theta$ relative to the surface normal after experiencing n-inelastic collisions. The partial escape distributions are the product of the path length distribution with the probability $W_n(s)$ for n-fold inelastic scattering as a function of the path length s, integrated over all possible path lengths,[18]

$$\phi_n(\mu,z') = \int_0^\infty Q(s,\mu,z')W_n(s)ds, \tag{1}$$

where the stochastic process for n-fold scattering in the quasielastic energy regime is given by[19]

$$W_n(s) = \left(\frac{s}{\lambda_i}\right)^n \frac{e^{-s/\lambda_i}}{n!}. \tag{2}$$

In the limiting case of small scattering parameters $\chi\to 0$, when the rectilinear motion model is applicable, the path length distribution resembles a delta function $Q(s,\mu,z')=\delta(s-z'/\mu)$ and the depth distribution functions are completely determined by the stochastic process,

$$\phi_n(\mu,z') = \left(\frac{z'}{\lambda_i\mu}\right)^n \frac{e^{-z'/\lambda_i\mu}}{n!}. \tag{3}$$

The partial escape distributions for the Si $2p$ transition excited by Mg $K\alpha$ radiation (soft x rays, photoelectron kinetic energy $E_{kin}\sim 1150$ eV) and the Si $1s$ line excited with 5295 eV photons (hard x rays, photoelectron kinetic energy $E_{kin}\sim 4080$ eV) are presented in Fig. 2 for $n=0-5$. The most striking difference between these two cases is the depth scale: the DDFs for hard x rays are seen to be much broader than for soft x rays by a factor of about 5. The hard x-ray DDFs are seen to approximately follow the Poisson formula [Eq. (3)]. The influence of elastic scattering is evident from the fact that the escape probability for electrons being inelastically scattered at least once does not vanish for $z'=0$. This is in contrast to Eq. (2) and is caused by electrons whose initial direction is directed toward the interior of the solid and that escapes after several deflections.

For a homogeneous solid, the area under the DDF curves represents the relative number of electrons that escape after n-inelastic collisions. These quantities are the so-called partial intensities $C_n(\mu)$,

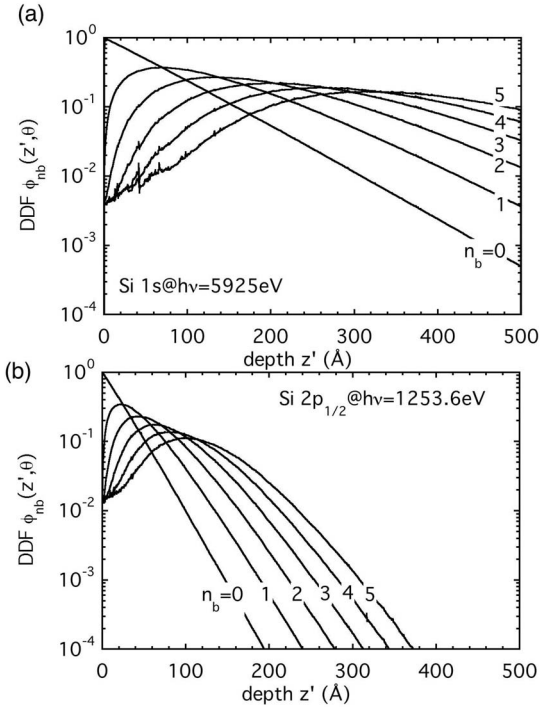

FIG. 2. Depth distribution functions $\phi_n(\mu,z')$, i.e., probability distribution for escape along the polar emission angle $\mu=\cos\theta$ after experiencing n-inelastic collisions inside the solid, for (a) the hard x-ray excited Si $1s$ spectrum and (b) the soft x-ray excited Si $2p$ spectrum (Ref. 27).

$$C_n(\mu) = \int_0^\infty \phi_n(\mu,z')dz'. \tag{4}$$

In particular, the intensity of the peak of electrons that escape without inelastic scattering (the no-loss peak in the photoemission spectrum) is equal to the area of the DDF for $n=0$, $I_{no\ loss}=C_0$. The higher order partial intensities correspond to the electrons winding up in the inelastic background. In the case of Si, where the inelastic losses are dominated by plasmon excitations, the higher order partial intensities are therefore equal to the intensity of the plasmon loss peaks of a given order.

The partial intensities reduced with the elastic peak intensity ($\gamma_n=C_n/C_0$) corresponding to the DDFs shown in Fig. 2 are displayed in Fig. 3. For a homogeneous solid, the first few ($n\lesssim 5$) reduced partial intensities $\gamma_n=C_n/C_{n=0}$ for X-ray photoemission spectroscopy (XPS) are given by the expression[15]

$$\gamma_n(\mu) = \kappa(\mu)^n, \tag{5}$$

where the quantity $\kappa(\mu)$ is given by

$$\kappa(\mu) = 1 - \frac{\omega/2}{1+\mu\sqrt{3(1-\omega)}},$$

and the single scattering albedo ω depends on the scattering parameter as $\omega=\chi/(\chi+1)$. When elastic scattering is negligible ($\lambda_{tr}\to\infty, \omega\to 0$), the partial intensities become independent of the scattering order,

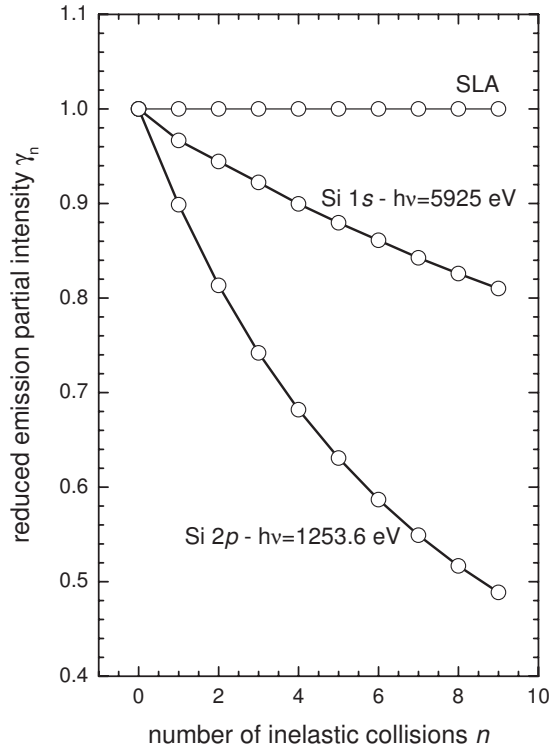

FIG. 3. Reduced emission partial intensities γ_n, i.e., the relative number of electrons escaping after experiencing a number n of collisions for the two spectra shown in Fig. 6. The line labeled "SLA" represents the partial intensities in the rectilinear motion model [straight line approximation (SLA)] when the partial intensities are independent of the collision number [see Eq. (2)].

$$\gamma_n(\mu) = 1,$$

as can also be seen directly by inserting the DDF in the rectilinear motion model [Eq. (3)] into Eq. (4) and performing the elementary integration.

In Fig. 3, it is indeed seen that for the hard x-ray case the partial intensities depend only weakly on the collision order: the intensity of the fifth plasmon loss peak is still 90% of the zero loss peak intensity, while for the soft x-ray case the fifth order plasmon loss peak is only 60% of the elastic peak intensity. Both sequences of partial intensities are seen to follow the power law [Eq. (5)], but for the hard x-ray case the value of κ is closer to unity since the influence of elastic scattering is weaker in this case. It is important to emphasize that this behavior is caused by the combined influence of elastic and inelastic scattering through the energy dependence of the scattering parameter χ and *not* by the increase of the absolute values of the path lengths with the photoelectron kinetic energy.

III. EXPERIMENTS

The hard x-ray experiments have been performed in a vacuum of about 1×10^{-7} Pa at the beamline ID16 of the European Synchrotron Radiation Facility of Grenoble (France) during a low current mode of the storage ring (four bunches). The experimental setup is identical to the one used in Ref. 12 and is described in detail in Ref. 5. Briefly, the incoming beam, set at $h\nu$=5925 eV, with a flux of about 2×10^{12} photons/s per 100 mA in the storage ring and a photon energy bandwidth of 340 meV, was impinging on Si at 45° from the sample surface. The sample, a piece cut from a commercial Si wafer, was placed with its surface perpendicular to the axis of the electron analyzer (normal emission). The analyzer, an electrostatic hemispherical spectrometer especially designed to detect high energy electrons,[5] was operated at a pass energy E_p of 60 eV, using an entrance slit of 1.6×25 mm^2. No cleaning procedure was performed in vacuum on the sample. The exit slit of the analyzer is defined by the spatial resolution of the two-dimensional detector (0.1 mm/channel). In the spectra presented here, we integrated the signal over 15 channels for an effective exit slit of 1.5 mm. Under these conditions, the expected analyzer resolution is ~470 meV, which, combined with the aforementioned photon bandwidth (and considering a Gaussian sum of the two), gives an overall expected energy resolution of 580 meV.

Mg $K\alpha$ excited Si $2p$ and $2s$ spectra were measured at the Vienna University of Technology using a 150 mm radius electrostatic hemispherical analyzer VG Microlab-300 (operated at a pass energy 50 eV), equipped with an unmonochromated Al-Mg twin anode source at a vacuum of approximately 10^{-8} Pa. The sample was cut from a commercial (lightly p-doped) Si wafer and was carefully cleaned by a few minutes of 3 keV Ar^+ sputtering until no traces of carbonaceous surface contamination were visible in the XPS spectrum.

The distribution of energy loss was extracted from reflection electron energy loss (REEL) spectra taken from measurements on another Si sample performed with the ESA-31 electron spectrometer based on a 180° hemispherical analyzer,[20,21] built at ATOMKI, Debrecen, with a 2.4 eV analyzer energy resolution (at 7 keV electron energy). During measurements, the vacuum in the sample chamber was better than 2×10^{-7} Pa. The primary electrons, at energies of 1500 and 4000 eV, hit the target perpendicularly, while the detector was placed at an emission angle of 70°.

IV. EVALUATION OF EXPERIMENTAL SPECTRA

For completeness, we present a brief synopsis of the method used to evaluate the experimental spectrum below. To extract the intrinsic spectrum from an experimental spectrum, one has to eliminate the features due to multiple inelastic scattering. This was achieved in the present work by means of the formula[22]

$$Y_k(E) = Y_{k-1}(E) - q_k \int_0^\infty L_{k-1}(T) Y_{k-1}(E+T) dT. \qquad (6)$$

Here, $Y_k(E)$ is the spectrum from which inelastic scattering has been removed to the $(k-1)$th order and the quantities L_k are the $(k-1)$-fold self-convolution of the energy loss distribution in an individual collision in the bulk $[w_b(T)]$ and at the surface $[w_s(T)]$. The coefficients q_k are functions of the partial intensities.[22] This formula can be applied consecu-

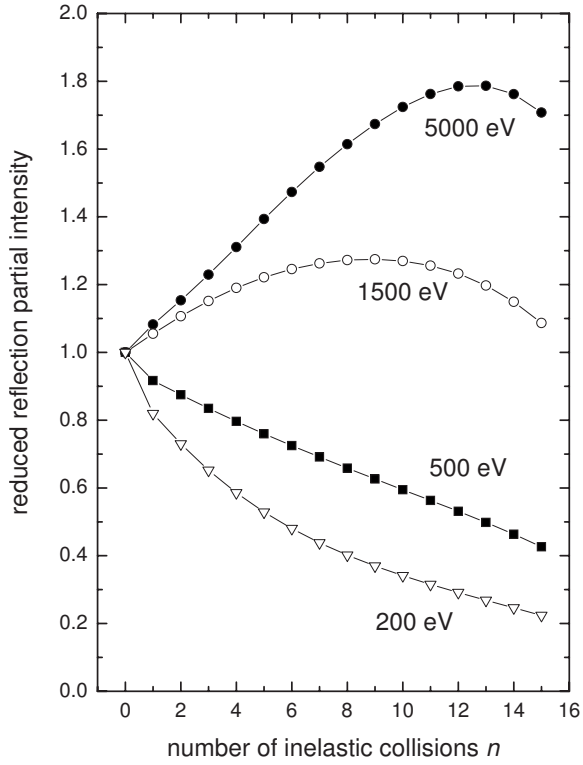

FIG. 4. Reduced partial intensities for reflection for various energies using the Mott cross section for elastic scattering (Ref. 26).

tively to eliminate multiple scattering features arising from different modes of the inelastic process, such as surface and bulk excitations,[14] and was also used to eliminate ghost lines arising from x-ray satellites when nonmonochromated x-ray sources are used, in particular, for the Si $2s$ and $2p$ spectra shown in Fig. 6(b) (see below). For the relative intensities of the satellite structures, the empirical results by Klauber[23] were used.

To find the distribution of energy losses T in individual collisions, $w_b(T)$ and $w_s(T)$, a simultaneous deconvolution of two loss spectra measured at different energies or geometrical configurations $y_{L,1}(T)$ and $y_{L,2}(T)$ can be performed using the formula[24]

$$w_b(T) = \sum_{p=0}^{\infty} \sum_{q=0}^{\infty} u^b_{p,q} y^{(p)}_{L,1}(T') \otimes y^{(q)}_{L,2}(T - T'),$$

$$w_s(T) = \sum_{p=0}^{\infty} \sum_{q=0}^{\infty} u^s_{p,q} y^{(p)}_{L,1}(T') \otimes y^{(q)}_{L,2}(T - T'), \qquad (7)$$

where the coefficients $u^b_{p,q}$ and $u^s_{p,q}$ are functions of the reflection partial intensities,[24] the quantities $y^{(p)}_{L,1}(T)$ and $y^{(p)}_{L,2}$ are the $(p-1)$-fold self-convolution of the spectra, and the symbol $\otimes$ denotes a convolution. The partial intensities for reflection calculated with a Monte Carlo model are presented in Fig. 4 for various energies, corresponding to the geometry given in the previous section.

Using these partial intensities, REEL spectra taken at 1500 and 4000 eV shown in Fig. 5(a) were subjected to the deconvolution procedure summarized in Eq. (7). The resulting distributions of energy losses in individual bulk $[w_b(T)]$ and surface $[w_s(T)]$ excitations are shown in Figs. 5(b) and 5(c), respectively. Note that the differential surface excitation probability exhibits a negative excursion at about 16 eV. This is a consequence of the so-called "begrenzungs" effect, i.e., the coupling between surface and volume scattering which implies that in the vicinity of the surface, the intensity of volume excitations is reduced at the expense of surface excitations.[24,25] The differential mean free path and surface excitation parameter shown in Fig. 5 along with the appropriate partial intensities were used for the deconvolution of the XPS spectra, employing Eq. (6).

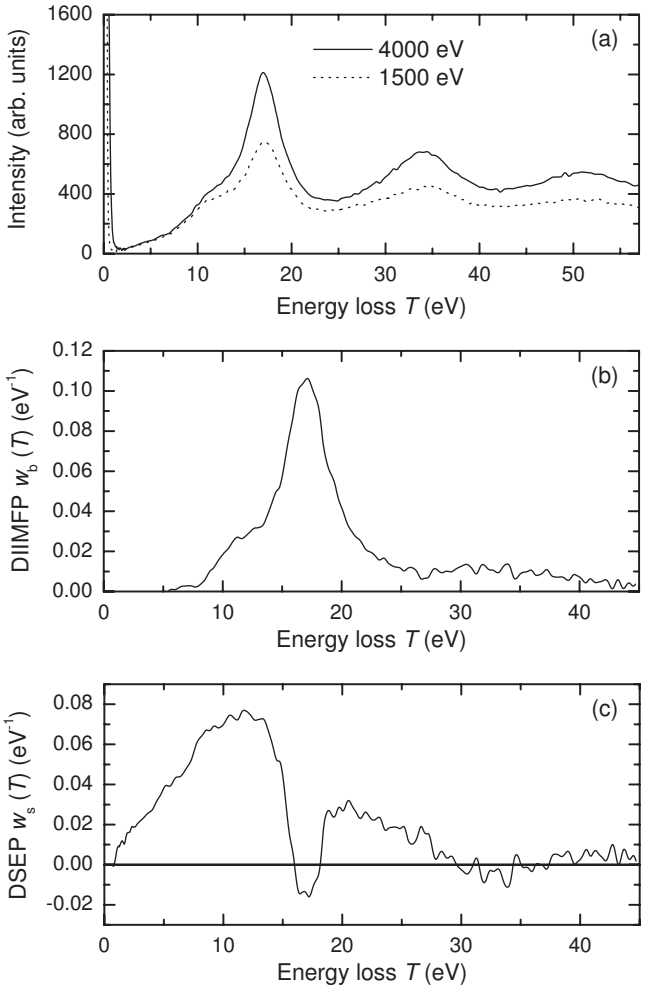

FIG. 5. (a) REELS spectra for 4000 and 1500 eV, (b) normalized differential inverse inelastic mean free path (DIIMFP) extracted from the data in (a), and (c) normalized differential surface excitation probability (DSEP) extracted from the data in (a).

The Monte Carlo model used to calculate the partial intensities[14] needs the inelastic mean free path and the differential elastic scattering cross section as input parameters. The resulting uncertainty in the partial intensities is mainly determined by the error in the inelastic mean free path, which is not well known, but estimated to be of the order of 10%–15%. However, for the deconvolution, the reduced partial intensities, i.e., the partial intensities divided by the in-

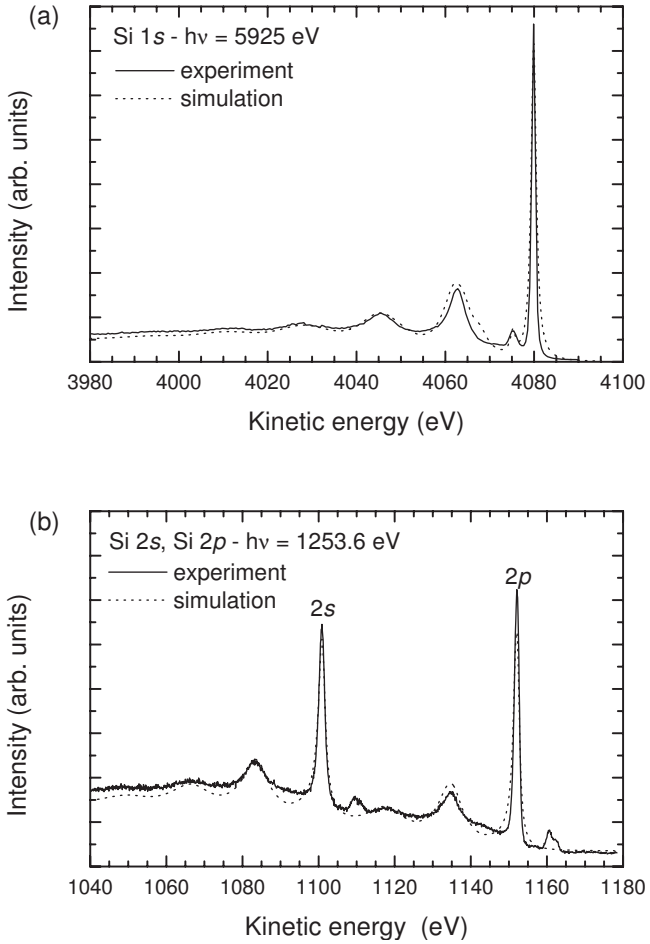

FIG. 6. (a) Hard x-ray excited photoelectron spectrum of the Si 1*s* line and (b) soft x-ray spectrum of the Si 2*s* and 2*p* lines. The dashed curves are results of simulations using the SESSA software (Ref. 27).

tensity of the no-loss peak, are required instead of the absolute partial intensities. In this case, the accuracy of the partial intensities is determined entirely by the accuracy of the elastic scattering cross section. The resulting accuracy in the reduced partial intensities is estimated to be better than 5% and is not expected to lead to a significant uncertainty in the contribution of the intrinsic scattering and other parameters derived from the analysis.

V. RESULTS AND DISCUSSION

Figure 6 shows the Si 1*s* hard x-ray (a) and the Si 2*s* and 2*p* soft x-ray (b) excited photoelectron spectra as solid lines. The dashed lines are results of SESSA simulations.[27] The hard x-ray excited photoelectron spectrum exhibits a small peak at 4.7 eV below the main photoelectron line that is due to the chemically shifted contribution of the passivation layer that is present on this sample and has a nominal thickness of about 8–10 Å. According to the initial bonding state model,[28] we interpret this peak as arising from the Si^{4+} chemically shifted contribution. The relative intensity of this peak in the simulation is consistent with the observed value. It is to be noted that the relative intensity of the oxide and elemental Si peak is sensitive to the value of the inelastic mean free path used in the simulation. This prompts us to conclude that the theoretical value for the inelastic mean free path of 78 Å used in the simulations (see Table I) is appropriate. The fact that this value is significantly higher than the results quoted in Ref. 12 for metallic samples and in Ref. 13 for Ge is consistent with higher values for the IMFP for medium energy electrons for Si compared to those for metallic samples or germanium.[29]

The number of plasmon loss peaks that can be discerned in this representation amounts to 4–5. A large number of plasmon loss peaks have also been reported in high energy photoemission studies using Cu $K\alpha$ radiation.[30] In the soft x-ray excited Si 2*s* and 2*p* spectra, small peaks are seen on the high energy side near the elastic photopeaks. These are due to the additional excitation of the Mg $K\beta_{3,4}$ x-ray satellite lines. The number of plasmon loss peaks seen in the soft x-ray excited photoelectron spectrum is smaller than that seen in the Si 1*s* spectrum. The ratio of the second to first plasmon loss peak is also clearly smaller than that for the Si 1*s* spectrum. These observations are completely consistent with the theoretical results in Figs. 2 and 3: while the partial intensities (which represent the relative intensities of the plasmon loss features as a function of the collision number) decrease rapidly with the scattering order for the Si 2*p* and 2*s* case, the decrease is much more moderate for the high energy Si 1*s* partial intensities. As outlined in Sec. II, this is *not* due to the larger escape depth for the high energy spectrum but is caused by the fact that elastic scattering is much weaker in the high energy case (the value of χ drops from 0.17 to 0.05 when going from 1000 to 5000 eV, see Table I).

The results of the deconvolution of multiple surface and bulk scattering from the hard x-ray excited photoelectron spectrum are shown in Fig. 7(a) as a dotted line. A pronounced plasmon loss peak remains in the background subtracted spectrum in the region between 4050 and 4070 eV. This is attributed to the creation of intrinsic plasmons. Assuming intrinsic excitations to follow Poisson statistics and assuming an intrinsic plasmon creation probability of ~30%, the contribution of intrinsic plasmons was eliminated from the spectrum and resulted in the spectrum represented by the thick solid line in Fig. 7(a). An expanded view of the resulting line shape is shown as open circles in Fig. 7(b), together with a fit of the peak shape to a linear combination of three Gaussian peaks, shown as the solid line. Besides the main peak close to 4080 eV, the component located at roughly 4075 eV is the chemically shifted contribution of the passivation layer. The third much smaller peak at lower kinetic energy is tentatively attributed to a further suboxide component. The width of the peaks amounts to 0.6 eV, in good agreement with the value expected on the basis of the experimental energy resolution.

The soft x-ray excited photoelectron spectrum was subjected to the same analysis, the only difference being that in the case of this unmonochromatized spectrum, Mg $K\beta_{3,4}$ satellite replicas were also eliminated with the same procedure (see Ref. 31 for details). The resulting background subtracted spectrum for the Si 2*p* peak is shown in Fig. 8(a). The contribution of intrinsic plasmons was clearly lower in this case

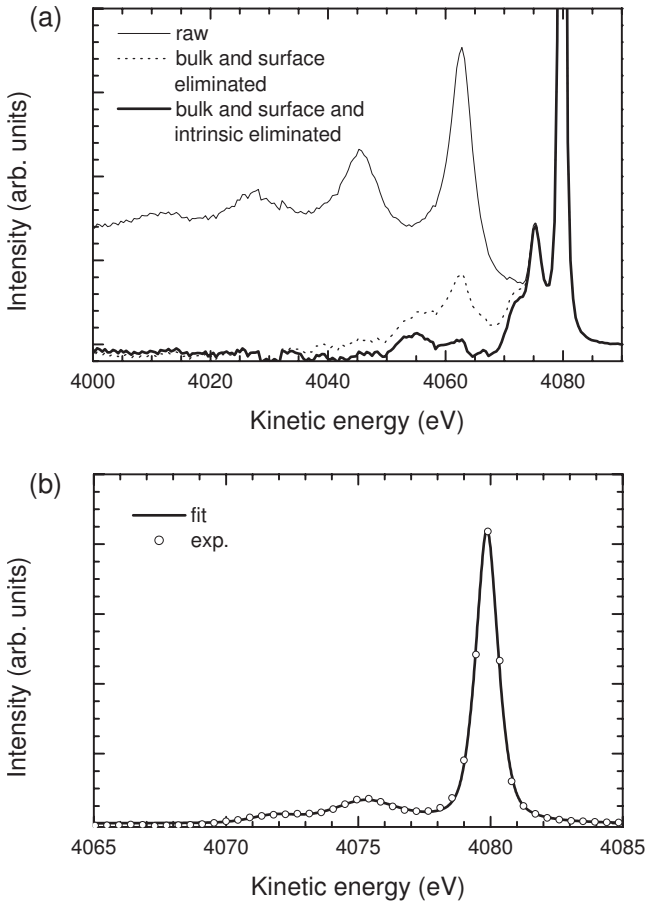

FIG. 7. (a) Deconvolution of the hard x-ray excited Si 1*s* spectrum and (b) fit of the resulting intrinsic line shape to a linear combination of three Gaussian peaks.

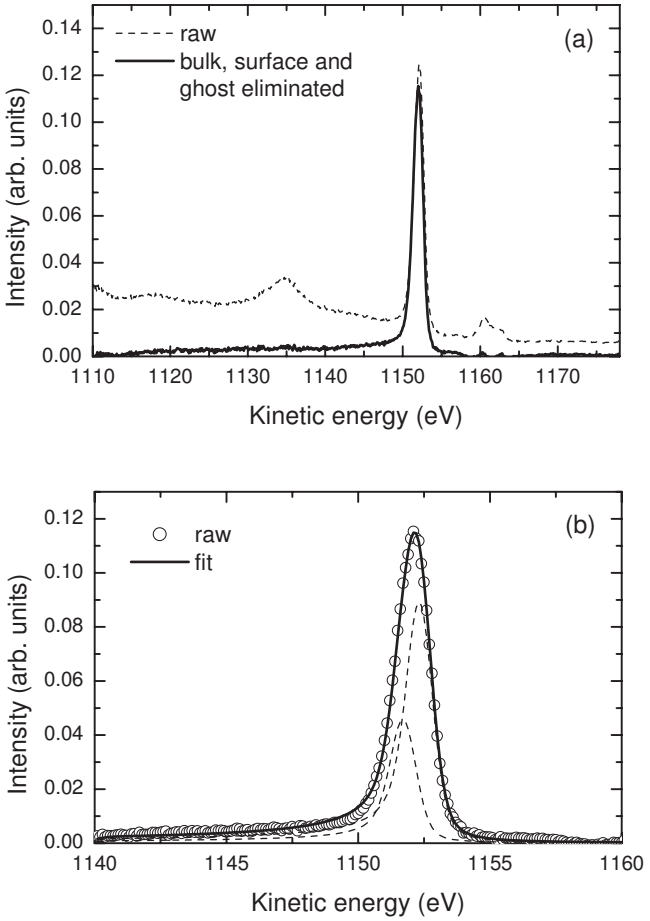

FIG. 8. (a) Deconvolution of the soft x-ray excited Si 2*p* spectrum and (b) fit of the resulting intrinsic line shape to a linear combination of two Doniach-Sunjic peaks.

and amounted to less than 10%. The resulting peak shape, shown in Fig. 8(b), is clearly asymmetric, in contrast to the Si 1*s* peak. The background subtracted peak was fitted by a linear combination of two Doniach-Sunjic lines, convoluted by a Gaussian that is taken to be representative for the experimental energy resolution. The two components are shown as dashed lines in Fig. 8(b). The solid line is the sum of the two components. The relative intensity of the $2p_{1/2}$ and $2p_{3/2}$ components amounts to 0.5, their energy separation was found to be $\Delta=0.62$ eV, in good agreement with earlier assessments,[32] the asymmetry parameter is $\alpha=0.10$, and their width is 0.4 eV.

In summary, the peak shape analysis of the hard and soft x-ray excited photoemission spectrum shows a clear asymmetry in the Si 2*p* spectrum, while the creation of intrinsic plasmons is low in this case. For the hard x-ray excited photoelectron spectrum, the opposite is observed: the line shape is symmetric, indicating that the creation of electron-hole pairs is weak in this case, but a strong intrinsic plasmon loss peak is observed [see the dotted line in Fig. 7(a)].

Within the three step model of photoemission, intrinsic excitations are conceived to occur when the sudden appearance of the core hole is screened by the solid state electrons. The resulting polarization field decelerates the outgoing photoelectron, giving rise to additional energy losses, the so-called intrinsic losses. This can lead to excitation of characteristic losses, for example, plasmon losses in nearly free electron materials, but can also lead to creation of electron-hole pairs, provided that the density of states near the Fermi level is sufficiently high. The latter condition is generally fulfilled in metals and also, as in the present work, for doped semiconductors. The probability for creation of electron-hole pairs is inversely proportional to the energy ω required to promote a loosely bound solid state electron over the Fermi edge: $\propto\omega^{-\alpha}$, where α is the singularity index.[33] Convoluting this loss distribution with a Lorentzian gives rise to the so-called Doniach-Sunjic asymmetric line shape[33] as observed in the 2*p* spectrum. In this respect, the absence of a clear asymmetry in the Si 1*s* hard x-ray spectrum due to electron-hole pair creation might appear as surprising. Since the 2*p* core level was measured by the more surface sensitive XPS, one tends to conclude that at surface we have a higher probability of electron-hole pair creation, and a lower one in the bulk. Actually, one cannot rule out that the presently observed asymmetry of the line shape of the Si 2*p* photoelectron peak has to be ascribed to surface core level shifted components, which have been reported, for soft x-ray excited 2*p* level, at both high and low kinetic energy sides of the main peak.[32,34] In general, the dependence of the total frac-

tion of intrinsic losses as well as the relative probability of characteristic losses and electron-hole pair creation on the photon energy and the binding energy of a particular shell has, to our knowledge, not been systematically studied, although the number of such studies is increasing recently.[35,36]

Regarding our results, the strong intrinsic plasmon loss peak following from the line shape analysis of the hard x-ray excited photoemission spectrum agrees with the picture where intrinsic plasmon creation in the photoemission process increases with increasing photoelectron kinetic energy.[37] Experimentally, Si 1*s* spectra taken at different photon energies of $h\nu$=3000 eV and $h\nu$=5500 eV show indeed that the ratio of the loss to the no-loss peak is enhanced at higher kinetic energy.[35] This was justified by the authors considering that at smaller kinetic energy (and electron velocity), the electrons in the solid have more time to relax, screening the field of the core hole more efficiently than at higher kinetic energy, where the probability of intrinsic plasmon creation becomes therefore higher. These results may be compared with a recent analysis on intrinsic and extrinsic excitations in HAXPES excited 1*s* and 2*s* core levels of Ge.[36] In particular, for the Ge 2*s*, at a kinetic energy of about 6.5 keV, the contribution from extrinsic excitation dominates the loss structure. However, a relatively high ratio of the intensity of the intrinsic excitations to the total intensity of the loss spectrum is reported, ranging from about 0.2 to about 0.4, depending on the spectrum analysis procedure employed.

A further phenomenon that complicates the interpretation of the results is the interference between extrinsic and intrinsic excitations.[38,39] Since emission of a photoelectron with an energy E_0 followed by an extrinsic energy loss ΔE contributes to the same final state as a photoelectron that suffered an intrinsic energy loss and is emitted with an energy $E_0-\Delta E$, quantum mechanical interference effects are expected for extrinsic and intrinsic loss processes in photoemission. Although the photoelectron kinetic energies used in the present work are rather high and interference effects are expected to be weak or negligible,[38,39] it is difficult to rule out any eventual influence of interference effects in our data since we cannot distinguish the contribution of extrinsic and intrinsic scattering in our experimental data.

VI. CONCLUSIONS

The true intrinsic line shapes of soft x-ray excited 2*p* and hard x-ray excited 1*s* core levels have been obtained by comparing experimental spectra with theoretical analysis. The comparison confirms the commonly employed theoretical model for the surface sensitivity of photoelectron spectroscopy over a wide range. Furthermore, the experimental spectra were deconvoluted to give the intrinsic line shape under the assumption that interference effects between intrinsic and extrinsic inelastic scattering are weak and can be neglected. For the high energy case, a more pronounced influence of intrinsic plasmon loss is observable, while there is no indication of an electron-hole pair creation, as evidenced by the symmetric shape of the peak. The intrinsic shape of the 2*p* core level indicates rather weak plasmon creation and exhibits an asymmetric shape.

ACKNOWLEDGMENTS

This work received financial support from the European Community under RTD Contract No. HPRI-CT-2001-50032. A.F., F.O., and P.T. acknowledge the European Community for granting their positions under the same contract. The valuable help of the staff at the ID16 beamline (ESRF) and the advices and the support of M. Grioni are gratefully acknowledged.

*Present address: European Synchrotron Radiation Facility, B.P. 220, F-38042 Grenoble, France.

[1] See Nucl. Instrum. Methods Phys. Res. A **547**, 1 (2005).
[2] See, for example, L. Braicovich, N. B. Brookes, C. Dallera, M. Salvietti, and G. L. Olcese, Phys. Rev. B **56**, 15047 (1997), and references therein.
[3] I. Lindau, P. Pianetta, S. Doniach, and W. E. Spicer, Nature (London) **250**, 214 (1974).
[4] J. J. Yeh and I. Lindau, At. Data Nucl. Data Tables **32**, 1 (1985).
[5] P. Torelli, M. Sacchi, G. Cautero, M. Cautero, B. Krastanov, P. Lacovig, P. Pittana, R. Sergo, R. Tommasini, A. Fondacaro, F. Offi, G. Paolicelli, G. Stefani, M. Grioni, R. Verbeni, G. Monaco, and G. Panaccione, Rev. Sci. Instrum. **76**, 023909 (2005).
[6] W. Drube, T. M. Grehk, R. Treusch, and G. Materlik, J. Electron Spectrosc. Relat. Phenom. **88-91**, 683 (1998).
[7] K. Kobayashi, M. Yabashi, Y. Takata, T. Tokushima, S. Shin, K. Tamasaku, D. Miwa, T. Ishikawa, H. Nohira, T. Hattori, Y. Sugita, O. Nakatsuka, A. Sakai, and S. Zaima, Appl. Phys. Lett. **83**, 1005 (2003); K. Horiba, M. Taguchi, A. Chainani, Y. Takata, E. Ikenaga, D. Miwa, Y. Nishino, K. Tamasaku, M. Awaji, A. Takeuchi, M. Yabashi, H. Namatame, M. Taniguchi, H. Kumigashira, M. Oshima, M. Lippmaa, M. Kawasaki, H. Koinuma, K. Kobayashi, T. Ishikawa, and S. Shin, Phys. Rev. Lett. **93**, 236401 (2004); M. Taguchi, A. Chainani, K. Horiba, Y. Takata, M. Yabashi, K. Tamasaku, Y. Nishino, D. Miwa, T. Ishikawa, T. Takeuchi, K. Yamamoto, M. Matsunami, S. Shin, T. Yokoya, E. Ikenaga, K. Kobayashi, T. Mochiku, K. Hirata, J. Hori, K. Ishii, F. Nakamura, and T. Suzuki, *ibid.* **95**, 177002 (2005).
[8] C. Dallera, L. Duò, L. Braicovich, G. Panaccione, G. Paolicelli, B. Cowie, and J. Zegenhagen, Appl. Phys. Lett. **85**, 4532 (2004).
[9] A. Sekiyama and S. Suga, J. Electron Spectrosc. Relat. Phenom. **137-140**, 681 (2004).
[10] S. Thiess, C. Kunz, B. C. C. Cowie, T.-L. Lee, M. Renier, and J. Zegenhagen, Solid State Commun. **132**, 589 (2004).
[11] G. Paolicelli, A. Fondacaro, F. Offi, G. Stefani, G. Cautero, M. Cautero, B. Krastanov, P. Lacovig, P. Pittana, R. Sergo, R. Tommasini, P. Torelli, M. Sacchi, M. Grioni, G. Monaco, and G. Panaccione, J. Electron Spectrosc. Relat. Phenom. **144-147**, 963 (2005); G. Panaccione, G. Cautero, M. Cautero, A. Fondacaro, M. Grioni, P. Lacovig, G. Monaco, F. Offi, G. Paolicelli, M. Sacchi, N. Stojić, G. Stefani, R. Tommasini, and P. Torelli, J.

Phys.: Condens. Matter **17**, 2671 (2005); G. Panaccione, M. Altarelli, A. Fondacaro, A. Georges, S. Huotari, P. Lacovig, A. Lichtenstein, P. Metcalf, G. Monaco, F. Offi, L. Paolasini, A. Poteryaev, M. Sacchi, and O. Tjernberg, Phys. Rev. Lett. **97**, 116401 (2006).

[12] M. Sacchi, F. Offi, P. Torelli, A. Fondacaro, C. Spezzani, M. Cautero, G. Cautero, S. Huotari, M. Grioni, R. Delaunay, M. Fabrizioli, G. Vankó, G. Monaco, G. Paolicelli, G. Stefani, and G. Panaccione, Phys. Rev. B **71**, 155117 (2005).

[13] Z. Berényi, B. Aszalós-Kiss, J. Tóth, D. Varga, L. Kövér, K. Tőkési, I. Cserny, and S. Tanuma, Surf. Sci. **566-568**, 1174 (2004).

[14] W. S. M. Werner, Surf. Interface Anal. **31**, 141 (2001).

[15] I. S. Tilinin and W. S. M. Werner, Surf. Sci. **290**, 119 (1993).

[16] W. S. M. Werner and I. S. Tilinin, Surf. Sci. **268**, L319 (1992).

[17] I. S. Tilinin, A. Jablonski, and S. Tougaard, Phys. Rev. B **52**, 5935 (1995).

[18] W. S. M. Werner, Surf. Interface Anal. **37**, 846 (2005).

[19] W. S. M. Werner, Phys. Rev. B **55**, 14925 (1997).

[20] L. Kövér, D. Varga, I. Cserny, J. Tóth, and K. Tőkési, Surf. Interface Anal. **19**, 9 (1992).

[21] W. S. M. Werner, L. Kövér, S. Egri, J. Tóth, and D. Varga, Surf. Sci. **585**, 85 (2005).

[22] W. S. M. Werner, Phys. Rev. B **52**, 2964 (1995).

[23] C. Klauber, Surf. Interface Anal. **20**, 703 (1993).

[24] W. S. M. Werner, Surf. Sci. **588**, 26 (2005).

[25] W. S. M. Werner, Surf. Sci. **526**, L159 (2003).

[26] A. C. Yates, Comput. Phys. Commun. **2**, 175 (1971).

[27] W. Smekal, W. S. M. Werner, and C. J. Powell, Surf. Interface Anal. **37**, 1059 (2005). See also http://www.nist.gov/srd/nist100.htm

[28] G. Hollinger and F. J. Himpsel, Phys. Rev. B **28**, 3651 (1983).

[29] S. Tanuma, C. J. Powell, and D. R. Penn, Surf. Interface Anal. **21**, 165 (1994).

[30] W. S. M. Werner, L. Kövér, J. Tóth, and D. Varga, J. Electron Spectrosc. Relat. Phenom. **122**, 103 (2002).

[31] W. S. M. Werner, T. Cabela, J. Zemek, and P. Jiricek, Surf. Sci. **470**, 325 (2001).

[32] P. Unsworth, J. E. Evans, P. Weightman, A. Takahashi, J. A. D. Matthew, and Q. C. Herd, Phys. Rev. B **54**, 286 (1996).

[33] S. Hüfner, *Photoelectron Spectroscopy* (Springer, Berlin, 1995).

[34] D. H. Rich, T. Miller, and T.-C. Chiang, Phys. Rev. B **37**, 3124 (1988).

[35] F. Yubero, L. Kover, W. Drube, Th. Eickhoff, and S. Tougaard, Surf. Sci. **592**, 1 (2005).

[36] L. Kövér, M. Novák, S. Egri, I. Cserny, Z. Berényi, J. Tóth, D. Varga, W. Drube, F. Yubero, S. Tougaard, and W. S. M. Werner, Surf. Interface Anal. **38**, 569 (2006).

[37] J. C. Fuggle, R. Lässer, O. Gunnarsson, and K. Schönhammer, Phys. Rev. Lett. **44**, 1090 (1980).

[38] L. Hedin, J. Michiels, and J. Inglesfield, Phys. Rev. B **58**, 15565 (1998).

[39] L. Hedin and J. D. Lee, J. Electron Spectrosc. Relat. Phenom. **124**, 289 (2002).